Global Biogeochemical Cycles

RESEARCH ARTICLE
10.1029/2020GB006646

Attributing Causes of Future Climate Change in the California Current System With Multimodel Downscaling

Evan M. Howard[1], Hartmut Frenzel[1], Fayçal Kessouri[2], Lionel Renault[3,4], Daniele Bianchi[3], James C. McWilliams[3], and Curtis Deutsch[1]

[1]School of Oceanography, University of Washington, Seattle, WA, USA, [2]Biogeochemistry Department, Southern California Coastal Water Research Project, Costa Mesa, CA, USA, [3]Department of Atmospheric and Oceanic Sciences, University of California Los Angeles, Los Angeles, CA, USA, [4]Laboratoire d'Études en Géophysique et Océanographie Spatiales, Université de Toulouse (joint with IRD, NCES, CNRS, UPS), Toulouse, France

Key Points:
- We dynamically downscale the response of the California Current System to climate changes from five global Earth System Models
- Stratification and remote chemical properties, rather than regional winds, play a decisive role in coastal biogeochemistry changes
- Oxygen decreases and temperature increases are robust across downscaled models, but the nutrient and productivity changes are not

Supporting Information:
- Supporting Information S1

Correspondence to:
E. M. Howard and C. Deutsch,
ehoward2@uw.edu;
cdeutsch@uw.edu

Citation:
Howard, E. M., Frenzel, H., Kessouri, F., Renault, L., Bianchi, D., McWilliams, J. C., & Deutsch, C. (2020). Attributing causes of future climate change in the California Current System with multimodel downscaling. *Global Biogeochemical Cycles*, *34*, e2020GB006646. https://doi.org/10.1029/2020GB006646

Received 24 APR 2020
Accepted 4 OCT 2020
Accepted article online 15 OCT 2020

Abstract Coastal winds in the California Current System (CCS) are credited with the high productivity of its planktonic ecosystem and the shallow hypoxic and corrosive waters that structure diverse macrofaunal habitats. These winds thus are considered a leading mediator of climate change impacts in the CCS and other Eastern Boundary Upwelling systems. We use an eddy-permitting regional model to downscale the response of the CCS to three of the major distinct climate changes commonly projected by global Earth System Models: regional winds, ocean warming and stratification, and remote water chemical properties. An increase in alongshore winds intensifies spring upwelling across the CCS, but this response is muted by increased stratification, especially during summer. Despite the seasonal shift in regional wind-driven upwelling, basin-scale changes are the decisive factor in the response of marine ecosystem properties including temperature, nutrients, productivity, and oxygen. Downscaled temperature increases and dissolved oxygen decreases are broadly consistent with coarse resolution Earth System Models, and these projected changes are large and well constrained across the models, whereas nutrient and productivity changes are small compared to the intermodel spread. These results imply that global models with poor resolution of coastal processes nevertheless yield important information about the dominant climate impacts on coastal ecosystems.

1. Introduction

The California Current System (CCS) is a physically dynamic and biologically productive eastern-boundary upwelling system (Harvey et al., 2017; Levin & Schwing, 2011). It is also expected to be a hotspot for ocean oxygen loss (Long et al., 2016) and ocean acidification (Gruber et al., 2012; Hauri et al., 2013) over the next century, with potentially dramatic consequences for marine ecosystems (Fabry et al., 2008; Keller et al., 2017; Koslow et al., 2011). A key limitation in forecasting climate change impacts in the CCS is uncertainty in determining how changes in ocean biogeochemistry imported from the broader Pacific basin may be ameliorated or exacerbated by regional forcing by winds or other coastal processes (Bakun et al., 2015; Di Lorenzo et al., 2005).

Seasonal alongshore winds contribute to upwelling of nutrient-rich water that not only supports high productivity in the CCS but also creates biologically stressful conditions for many organisms by drawing low dissolved oxygen and acidified water onto the continental shelf (Adams et al., 2013; Chan et al., 2008; Feely et al., 2008). Because of the potential impact of changing winds on upwelling and coastal biogeochemistry, changes to the intensity and timing of alongshore winds have been a major focus of prior work on climate change in the CCS. Much of this work stems from the hypothesis that differential warming over land versus ocean will enhance surface pressure gradients and the alongshore wind stress that is favorable for coastal upwelling (Bakun, 1990). Subsequent analyses of observational data and global Earth System Model (ESM) output in eastern boundary upwelling systems globally have largely focused on refining and testing this hypothesis, leading to the expectation of poleward shifts in the peak intensity of alongshore winds (Rykaczewski et al., 2015; Sydeman et al., 2014). However, in the CCS in particular, shifts in upwelling-favorable winds by 2100 may be less significant than in other eastern boundary systems

(Wang et al., 2015), and apparent trends in the observational record may represent natural variability rather than evidence of shifting wind patterns (Brady et al., 2017).

Despite this longstanding emphasis on coastal winds, the response of physical, biogeochemical, and ecosystem properties to climate change in the CCS remains ambiguous. The cross-shore wind drop-off has a substantial influence on coastal productivity and can modulate regional rates over time even if peak off-shore winds remain unchanged (Renault, Deutsch, et al., 2016). The seasonal cycle of winds may also be changing; when upwelling velocity is evaluated directly in ESM output, spring intensification may be counterbalanced by decreases across the rest of the upwelling season (Brady et al., 2017). Increasing stratification with rising temperatures may offset increases in upwelling-favorable winds (García-Reyes et al., 2015) and alter basin scale nutrient distributions such that nutrient supply to the surface CCS may be enhanced (Rykaczewski & Dunne, 2010; Xiu et al., 2018). In general, the contributions of multiple drivers to changing CCS biogeochemistry have not been individually quantified. Further, while climate forcings from individual ESMs have been downscaled into regional models which resolve some coastal processes (Gruber et al., 2012; Hauri et al., 2013; Xiu et al., 2018), biogeochemical responses are highly variable across commonly used ESMs, more so than the internal climate variability within individual ESMs (Alexander et al., 2018; Brady et al., 2017). Thus, downscaled results from a single ESM may not represent a robust or representative future projection.

In this work, we assess the biogeochemical response of the CCS to distinct climate change forcings across five dynamically downscaled ESMs. Specifically, we conduct experiments to isolate the effects on CCS climate responses of three major drivers of coastal change: (1) remote (basin scale) changes in biogeochemical variables (nutrients and O_2), (2) density stratification by both remote and regional surface heat and freshwater fluxes, and (3) regional winds within the CCS. The global scale ESM climate forcings are downscaled through a single high-resolution Regional Ocean Modeling System framework (Shchepetkin & McWilliams, 2005). Biogeochemical responses are linked through a shared ecosystem model, the Biogeochemical Elemental Cycling model (Moore et al., 2002)—hereafter the ROMS-BEC model. We evaluate model output for upwelling velocity (w), temperature (T), dissolved nitrate (NO_3^-) and oxygen (O_2) concentrations, and net primary productivity (NPP; rates of net autotrophic production available to support the CCS ecosystem). O_2 in particular is a key ecosystem variable and biogeochemical tracer that is rarely evaluated in regional simulations of the future CCS (Dussin et al., 2019; Howard et al., 2020). We take this approach in order to distinguish which mechanisms are most important in driving changing biogeochemistry and to identify whether changes in the specific evaluated variables are well constrained in the future CCS.

2. Methods

2.1. Configuration

The ROMS-BEC simulations span the Northeast Pacific ocean from 15°N to 60°N and from the North American coast to roughly 4,000 km offshore, with hindcast years 1994–2007 at monthly resolution. The model grid has 322 offshore cells and 450 alongshore cells for a horizontal resolution of 12 km and 42 vertical levels with terrain (i.e., bathymetry) following coordinates. The numerical models, configuration, and boundary conditions are as described in Renault et al. (2020) and Deutsch et al. (2020); the 4 km model presented in those works covers a subset of the 12 km model domain presented here.

In brief, horizontal boundary and initial conditions for temperature, salinity, horizontal velocity, and sea surface elevation are taken from the Mercator global ocean reanalysis (GLORYS2V3; http://marine.copernicus.eu/) and interpolated to the ROMS-BEC model grid as a function of depth. Surface evaporation, heat, and momentum fluxes are estimated from bulk formulae (Large, 2006), and atmospheric conditions including air-temperature at the sea surface, precipitation, and downwelling radiation are derived from uncoupled Weather Research Forecast model output (c3.6.1; Skamarock et al., 2008) as in Renault, Hall, et al. (2016) and Renault et al. (2020). Feedbacks between winds and mesoscale currents are parameterized as a linear function of the surface wind stress as in Renault, Molemaker, et al. (2016) in order to avoid the computational cost of a fully coupled ocean-atmosphere model. This linear relationship is observationally supported in the CCS (Renault et al., 2017). River runoff is derived from Dai et al. (2009) and is added offline as surface precipitation at the coast. While rivers and estuarine exchange circulation north of ~40°N are important

physical and biogeochemical features of the nearshore CCS (Davis et al., 2014; MacCready et al., 2009; Siedlecki et al., 2014), the 12 km ROMS-BEC model does not include detailed representation of individual river plumes and associated biogeochemical fluxes or water exchanges with the Salish Sea, potentially leading to underestimation of local stratification and lateral nutrient inputs in the northern CCS.

The model representation of the planktonic ecosystem and associated biogeochemical transformations includes three phytoplankton functional groups, a single class of zooplankton, and particulate and dissolved organic matter, nitrogen, silica, phosphorus, and iron coupled via fixed phytoplankton stoichiometry. The ecosystem model is linked to an ocean biogeochemistry module that includes water column and sediment biogeochemical cycling, including that of carbon and oxygen. Parameterizations for particle remineralization, gas exchange, sediment fluxes, and other fluxes are detailed in Deutsch et al. (2020).

2.2. Validation

The 12 km resolution model hindcasts are in good agreement with climatological observations from the World Ocean Atlas (Figure S1; Garcia et al., 2013a, 2013b; Locarnini et al., 2013; Zweng et al., 2013). Both mesoscale and submesoscale processes play important roles in modulating nutrient supply and primary productivity in the coastal CCS. In particular, mesoscale filaments and eddies lead to subduction and offshore transport of offshore waters (Gruber et al., 2011; Nagai et al., 2015), which can limit nearshore NPP. Submesoscale mixing similarly enhances eddy removal of nearshore nutrients and organic matter during seasonal upwelling, but by redistributing nutrients offshore and enhancing vertical transport can stimulate offshore production (Kessouri et al., 2020; Li et al., 2012). We report results averaged from 0–200 km offshore, broadly encompassing the range over which these processes may reduce the offshore gradients in nutrient supply and NPP and resulting vertical redistribution of biogeochemical variables by the biological pump. Biases related to resolution of these (sub)mesoscale processes are shared across the downscaled ESMs.

While few data sets exist at the appropriate scales of space and time to evaluate the impact of missing (sub) mesoscale processes across the CCS model domain (Capet et al., 2008), the closely related 4 km resolution ROMS-BEC model has been extensively validated against available observational data for a broad suite of ocean physical and biogeochemical fields. It demonstrates a high fidelity in reproducing observations of the mean state, variability, and trends of key tracers including temperature, nutrient concentrations, NPP, and dissolved O_2 (Deutsch et al., 2020; Renault et al., 2020). Beyond the broad agreement between observations and both the 4 and 12 km resolution hindcasts, downscaled climate projections from both model resolutions agree well. Differences are dominated by mesoscale variability rather than systematic spatial differences (Figure S1). An exception is NPP, which has a broader band of nearshore productivity in the 12 km model than in the 4 km model; for example, near Cape Mendocino where this difference is largest, surface NPP in the 12 km resolution hindcast is roughly 35% lower nearshore and 20% higher offshore than in the 4 km hindcast (Figure S2). However, comparisons of the 4 km resolution hindcast with a nested 1 km model in the central CCS suggest that permitting submesoscale processes may dampen the offshore productivity gradient (Kessouri et al., 2020), which would largely compensate the observed differences between the 12 and 4 km models. The weaker 12 km model productivity gradient may contribute to projected stronger summer decreases offshore, with the result that depth-integrated NPP is 3.5% lower (0–200 km offshore) in the 12 km projections than in the equivalent 4 km projection (Figure S2). Regardless of this caveat, the regional 100 year climate anomalies for all variables, including NPP, are not significantly different between resolutions (Figure S3; Table S2). This agreement suggests that we can capture key downscaled climate responses through the less computationally expensive 12 km resolution model, which also covers a greater latitudinal range than the 4 km domain.

2.3. Downscaling

To downscale the climate change signals in the CCS, we rerun the hindcast simulations with the addition of climate forcing anomalies. The anomalies are generally constructed from epoch differences between 2071–2100 and 1971–2000 climatological conditions (hereafter referred to as 2100–2000) from the coarse resolution global fields of tracers and surface forcings from five ESMs (Table 1) from the Coupled Model Intercomparison Project (CMIP5; Taylor et al., 2012) using Representative Concentration Pathway 8.5 ("business as usual"). Boundary forcings are interpolated to the ROMS-BEC model grid, and downscaled

Table 1
Description and Abbreviations of Earth System Models, Climate Forcing Experiments, and Variables Presented in This Work

Earth System Model (ESM)	Abbreviation
National Oceanic and Atmospheric Administration Geophysical Fluid Dynamics Laboratory, GFDL-ESM2M	GFDL
Met Office Hadley Centre and Insituto Nacional de Pesquisas Espaciais, HadGEM2-ES	HAD
Institut Pierre-Simon Laplace, IPSL-CM5A-LR	IPSL
Max-Planck-Institut für Meteorologie, MPI-ESM-LR	MPI
National Science Foundation - Department of Energy - National Center for Atmospheric Research, CESM1(BGC)	NCAR
Average response across ESMs	Avg
Response from multi-model ensemble mean of ESM forcings	Ens

Climate forcings				
Interpolated: ESM outputs interpolated onto ROMS-BEC grid	Downscaled: ESM 2071–2100 to 1971–2000 anomalies added (✓) to ROMS-BEC hindcast			
	Fully forced, SBW:	Stratification, S:	Biogeochemistry, B:	Winds, W:
	Lateral boundary forcings and initial interior conditions			
(1) T, S	✓	✓		
(2) Nutrients, O_2, carbonate system[a]	✓		✓	
	Atmospheric forcings			
(4) pCO_2	✓		✓	
(5) Radiation, humidity, T, heat fluxes[b]	✓	✓		
(6) Windspeed[c]	✓			✓

Climate projections and anomalies in physical and biogeochemical variables presented						
Upwelling	Salinity	Temperature	Photosynthetically available radiation	Nitrate	Net primary productivity	Oxygen
w	S	T	PAR	N	NPP	O

[a]Specifically, biogeochemical anomalies include concentrations of dissolved nitrate, phosphate, silicate, iron, oxygen, dissolved inorganic carbon, and total alkalinity. The HAD model does not report changes in phosphate; because phosphate does not limit productivity in the CCS, this forcing was estimated as 1/15th the change in nitrate. [b]Radiation fluxes include long and shortwave radiation, and changes are expressed as ratios of 2100/2000 fluxes instead of differences. Evaporation, latent heat flux, and sensible heat flux are calculated from other property anomalies using bulk formulae (Large, 2006; Renault et al., 2020). No precipitation anomalies are applied; changes in precipitation and the freshwater balance are poorly constrained across ESMs, and associated freshwater fluxes are consistent in direction with evaporation but too small in magnitude to significantly affect the downscaling results. [c]No wind changes are applied for the NCAR downscaling; NCAR wind fields are reported as wind stress only, and conversion of wind stress to wind speed is anticipated to result in additional uncertainties without qualitatively changing the results of the analysis.

future projections are initialized with the 100-year climate anomalies added to WOA climatological initial conditions within the model grid. No spin-up period was used—including or removing the first 1–4 years of model output does not affect upper ocean climatologies considered in this work, nor do the ESM and downscaling anomalies systematically diverge over the time span of the run in the upper ocean and coastal portions of the model domain we present. This consistency indicates that ROMS-BEC interior conditions rapidly respond to external forcings, and the downscaling duration is sufficiently long to detect climatological differences in model responses.

Changes in the lateral boundary conditions from each ESM include climatological anomalies in salinity, temperature, nutrient and oxygen concentrations, and carbonate system parameters (Table 1). Changes in surface forcings expected to alter stratification include long-wave and short-wave radiation, and sensible and latent heat estimated from anomalies in near-surface air temperature and evaporation via bulk formulae as in the hindcast (Large, 2006). Radiative forcing changes only were derived from the epoch ratio instead of differences.

We do not apply changes to precipitation or river freshwater inputs as surface forcings within the ROMS-BEC domain but do apply salinity boundary forcing anomalies that result in part from basin scale hydrologic cycle changes in the ESMs. Local climate and human use driven changes in freshwater inputs to the CCS are poorly constrained (particularly river inputs; e.g., Arora & Boer, 2001; Ferrari et al., 2007; Morrison et al., 2002; Naik & Jay, 2011; Pytlak et al., 2018), and we expect basin scale anomalies and local warming to drive greater density and stratification changes over the CCS (Capotandi et al., 2012) than

local river and precipitation changes. Neglecting freshwater input changes could underestimate increased stratification, particularly in the northern coastal CCS, but downscaled salinity changes are not significantly less negative than the CMIP5 anomalies including local hydrologic changes (Supporting Information S1).

In order to evaluate biologically relevant differences in light fields, surface downwelling shortwave radiation is multiplied by a factor of 0.45 to convert to photosynthetically available radiation (PAR; e.g., Gould et al., 2019). Changes in surface momentum fluxes associated with winds are included for four of the five ESMs. NCAR model output in the CMIP5 archive includes wind stress but not the windspeed fields used to force circulation and other processes in the ROMS-BEC model. Thus, the NCAR model forcings are downscaled without any 100 year change in winds, but the downscaling approach is otherwise identical to the other ESMs. In addition to downscaling individual global ESMs, we average climate forcings across all five ESMs and apply this average to generate a downscaled multimodel ensemble mean-forcing case (hereafter "ensemble") projection. These dynamically downscaled results are compared to ESM results directly interpolated to the ROMS-BEC model grid without downscaling.

2.4. Experimental Design

Downscaled projections are generated from all the climate forcings from each ESM, including changes in heat and freshwater fluxes that collectively contribute to altered density structure and upper water-column stratification, basin scale changes in biogeochemistry, which propagate into the CCS, and changing near-surface winds (Table 1). Projections with the combined effects of these climate forcings are referred to as the stratification, biogeochemistry, and winds (SBW) case. In order to isolate and attribute changes due to each of these, we separately conduct the following three experiments: First, only the boundary conditions and surface forcings impacting stratification are varied according to the ESM 2100–2000 climate anomalies (S case), and other boundary and interior conditions remain as in the hindcast. Second, only remote biogeochemical boundary conditions, including nutrients and O_2, are changed (B case). Finally, only surface winds are changed (W case). As with the SBW projection, each experiment is conducted separately for the five ESMs evaluated as well as the ensemble case in which the downscaling is driven by the averaged climate forcings across ESMs (six simulations per case). Additionally, the remote (lateral boundary and initial interior conditions) and local (atmospheric forcing over the model domain) contributions to stratification are separately evaluated for the ensemble average case.

2.5. Averaging

Monthly climatologies of the hindcast, projections, and 100 year differences are generated from the 14-year time series for each model cell and variable. Regional averages for the CCS are then calculated from 0–200 km offshore, normal to the coast. This offshore range is comparable to prior work on the influence of coastal upwelling and offshore transport on biogeochemical fluxes (100 to >500 km; Brady et al., 2017; Gruber et al., 2011; Nagai et al., 2015; Wang et al., 2015; Xiu et al., 2018) and encompasses key physical and ecosystem bounds over most of the CCS, including the continental shelf and observed offshore limits of many coastal species. Restricting the analysis to closer to shore (e.g., 100 and 50 km) shifts the magnitude of projected changes, but not the general conclusions of this work with regard to the significance of those changes and the key underlying climate forcings.

We analyze the CCS region extending from the southern tip of the Baja California Peninsula to the southern tip of the Haida Gwaii Archipelago, 22.9–52°N. We report results for the southern CCS (22.9–34.45°N, Point Conception), the central CCS (34.45–40.44°N, Cape Mendocino), and the northern CCS (40.44–52°N). These latitudinal ranges are operationally defined based on geographical features and the variable extent of the California Current and California Undercurrent (e.g., Gómez-Valdivia et al., 2015; Lynn & Simpson, 1987; Sydeman et al., 2011; Supporting Information S1).

2.6. Statistical Tests

We evaluate whether the projections differ from the hindcasts across the range of global scale and downscaled ESMs (null hypothesis of no difference between projections and hindcasts). We also evaluate whether the 100 year changes diverge between ESMs and downscalings (null hypothesis of no difference between interpolated and downscaled ESMs). We use the nonparametric paired Wilcoxon signed-rank test to identify differences in the intermodel median that are potentially robust across the intermodel range ($\alpha = 6.25 \times 10^{-2}$, the minimum value possible with $n = 5$). While deviations from normal error

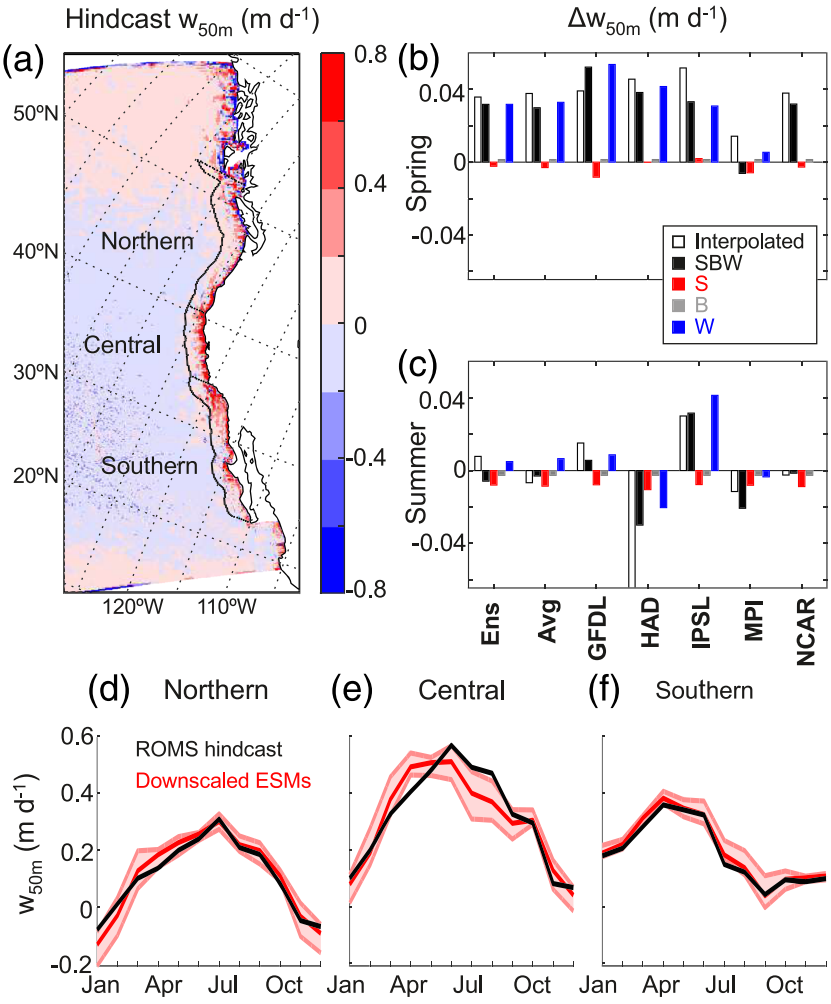

Figure 1. Upwelling velocity at 50 m depth (w_{50m}). (a) Map of hindcast (1994–2007) annual average from ROMS-BEC. Black alongshore contours indicate 0–200 km offshore regions of the California Current System (CCS) averaged for remaining panels. (b) 2100–2000 change (Δ) in spring (March–May), averaged over the coastal CCS, for global Earth System Models (ESMs) and downscalings: These include both the average response across individual models (Avg) and the separate multimodel ensemble mean forcing case (Ens). See Table 1 for full description of abbreviation for models (*x*-axis groups) and climate forcings (colored bars within groups). Regional wind forcing (W; blue) is generally large enough to explain the overall springtime response of w_{50m} (SBW; black) in the multimodel ensemble forcing as well as the individual downscaled ESMs, but stratification (S; red) can moderate the overall response in some models. (c) Summer (June–August) Δ. On average, stratification forcing is similar in magnitude to wind forcing. (d–f) Monthly climatologies of hindcast and downscalings with full climate forcing (SBW), for the northern, central, and southern CCS regions. The intermodel range of the downscalings is shaded (red).

distributions cannot be reliably assessed (for $n = 5$), we also calculate the paired Student's t test for each comparison—in nearly all comparisons with $p_W = 6.25 \times 10^{-2}$ from the nonparametric test, $p_t \leq 5 \times 10^{-2}$ from the parametric test. Cases where the two tests agree are identified as robust climate anomalies. These are presented in the results (p_t is reported), while every regional and CCS-wide test is presented in full in Table S1. Nonparametric confidence intervals are not distinguishable from the intermodel range, so the mean and range of 100-year anomalies are reported.

3. Results and Analysis

We first present upwelling velocity at 50 m depth (w_{50m}, m s^{-1}), as this variable has been an important focus of prior research on the climate response of the CCS. We next present results for temperature at 100 m

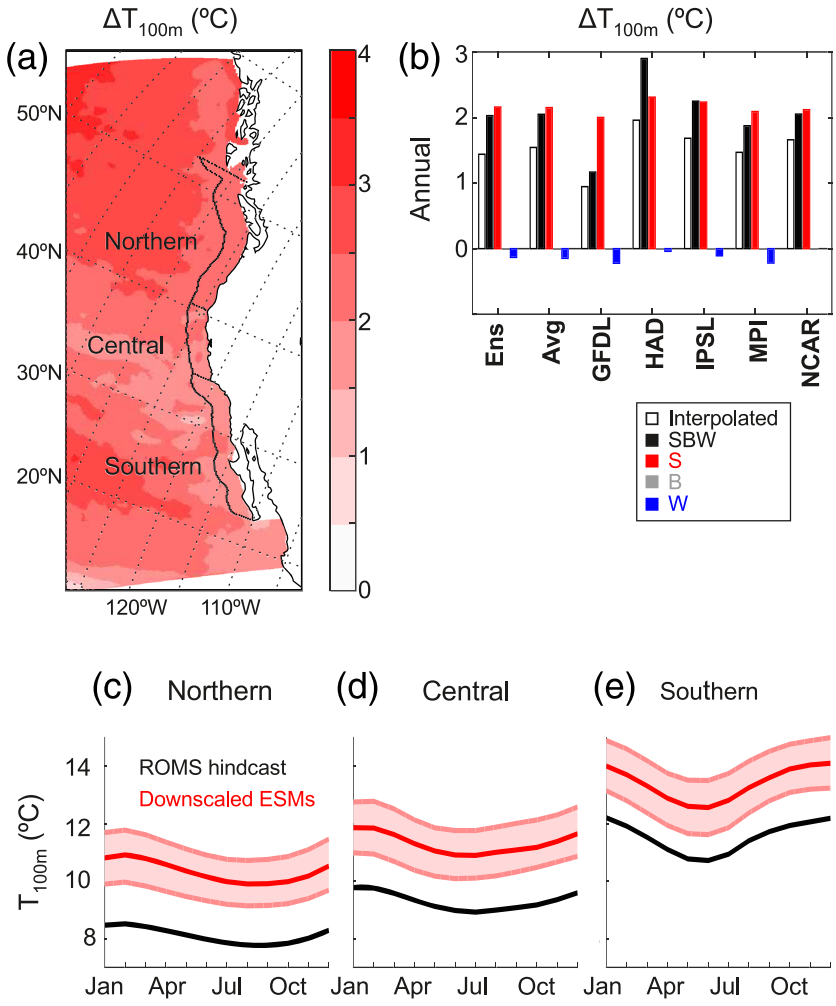

Figure 2. Temperature at 100-m depth (T_{100m}). (a) Map of 2100–2000 change (Δ), annual average in ensemble mean forcing case. (b) Annual average 2100–2000 change (Δ), averaged over the coastal CCS. The stratification forcings (S; red), including heating changes, are large enough to explain the overall response of T_{100m} (SBW; black), but regional winds have a minor cooling effect (W; blue). (c–e) Regional monthly climatologies of hindcast and downscalings with full climate forcing (SBW).

(T_{100m}, °C) and NO_3^- at 100 m (N_{100m}, mmol m^{-3}); a depth of 100 m is below the base of the surface mixed layer (seasonally roughly 10–70 m) and near the base of the seasonal nutricline over most of the coastal CCS. Thus, changes in N_{100m} are expected to primarily reflect climate forcings which change the supply of nutrients to the surface during upwelling, rather than the influence of primary production at shallower depths. Fourth, we present NPP integrated over the euphotic zone (NPP_z, mmol C m^{-2} y^{-1}; to depth of 1% of incident PAR. Finally, we present O_2 at 200 m (O_{200m}, mmol m^{-3}), which is influenced by both the physical and ecosystem dynamics of the system and has rarely been examined in simulations of the future CCS. A 200 m depth approximates the outer continental shelf and base of the oxycline over much of the CCS. Salinity and PAR changes are small. PAR is discussed briefly in the context of changing NPP, and these results are otherwise included in Figures S4 and S5.

For each variable, we present climatological annual mean maps of downscaled projected centennial climate anomalies, hereafter denoted Δ (such that $\Delta X = \bar{X}_{projection} - \bar{X}_{hindcast}$, where the monthly climatologies from the hindcast and projections are averaged to generate a mean climatological year for each period). The exception is upwelling—Δw_{50m} is small on an annual basis, and so we illustrate spatial variability in the hindcast. We also plot the CCS-average anomalies (0–200 km offshore) for each experimental case, as well as regional monthly climatologies of hindcast and projected conditions.

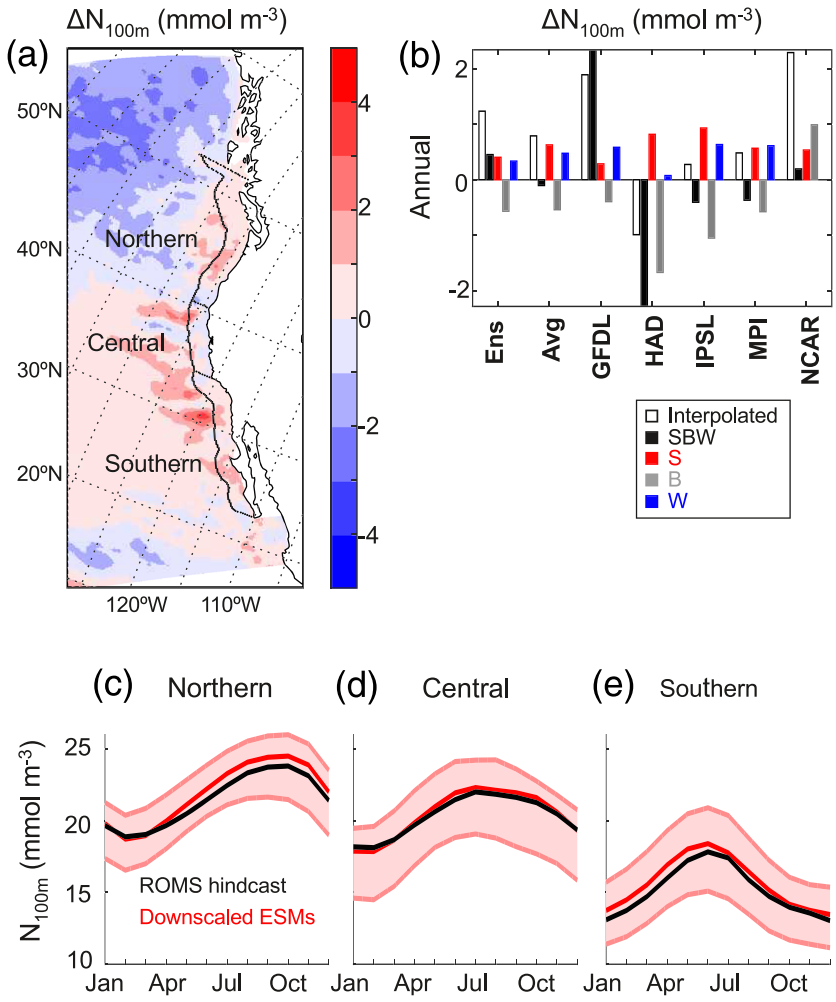

Figure 3. Nitrate concentrations at 100-m depth (N_{100m}). (a) Map of 2100–2000 change (Δ), annual average in ensemble mean forcing case. (b) Annual average 2100–2000 change (Δ), averaged over the coastal CCS. Biogeochemical boundary conditions (B; gray) and stratification (S) generally cause changes as large as or larger than winds (W). (c–e) Regional monthly climatologies of hindcast and downscalings with full climate forcing (SBW).

3.1. Upwelling Velocity

Hindcast w_{50m} (Figure 1a) and projected w_{50m} vary latitudinally across the CCS, with the most seasonally uniform rates to the south and greater seasonality and later annual peaks in upwelling farther north (Figures 1d–1f). The Δw_{50m} are small on an annual basis (mean 0.005 m d^{-1}, −0.010 to 0.023 m d^{-1} range across downscaled models) and similar between the interpolated (global scale) and downscaled ESM results (Figures 1b and 1c) from 0 to 200 km offshore. Models are also compared for the 0–100 km offshore area where wind stress driven upwelling is strongest and wind stress curl less important (Figure S6; comparable to the 1° longitude limits used by Wang et al., 2015, and Brady et al., 2017).

As expected from prior work, our results identify springtime intensification of upwelling by 2100 in the central and northern CCS (Figures 1d and 1e)—peak upwelling shifts earlier in the year. However, compensating decreases in upwelling in the summertime central CCS and increased winter downwelling in the northern CCS lead to little change in net annual velocities compared to the intermodel variability; no robust intermodel climate anomalies in net annual upwelling are identified anywhere in the coastal CCS.

Comparing forcing mechanisms, wind changes (W) are an important driver of enhanced springtime upwelling. On an annual basis, and in spring in particular, the results of the full forcing SBW downscalings are on

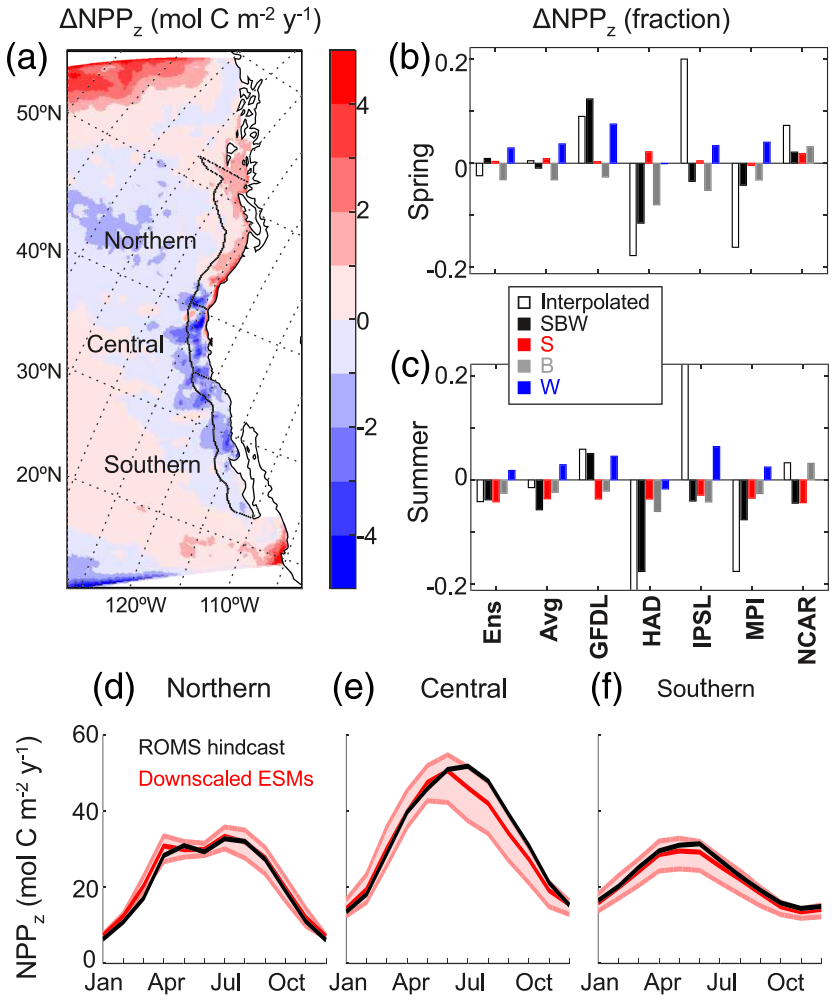

Figure 4. Net primary productivity integrated over the euphotic zone (to 1% of incident photosynthetically available radiation; NPP_z). (a) Map of 2100–2000 change (Δ), annual average in ensemble mean forcing case. (b) 2100–2000 change (Δ) in spring (March–May) and (c) summer (June–August), averaged over the coastal CCS. Biogeochemical boundary conditions (B) and stratification (S) generally cause changes as large as or larger than winds (W); stratification changes generally increase spring productivity and decrease summer productivity. (d–f) Regional monthly climatologies of hindcast and downscalings with full climate forcing (SBW).

average within 5% of those from wind forcing alone (Figure 1b). However, increasing stratification (S) is an important compensating factor that generally decreases upwelling in the summertime northern and southern CCS and both spring and summer in the central CCS, even when the analysis is restricted to nearshore areas with the greatest wind stress driven upwelling (0–100 km offshore; Figure S6). Both regionally and CCS wide, the SBW projections are roughly equivalent to the sum of the W and S anomalies for the four downscaled models in which the W case is evaluated, suggesting that those two forcings interact in a nearly linear manner to force the overall climate response.

3.2. Temperature

Projected ΔT_{100m} are similar throughout the year and increase with latitude in the coastal CCS (Figure 2). Temperature increases are significant compared to the intermodel variability for both the ESMs (mean 1.5°C, 0.9–2.0°C range across models; $p_t = 7.9 \times 10^{-4}$) and downscaled models (mean 2.0°C, 1.2–2.9°C range; $p_t = 1.9 \times 10^{-3}$). The downscaled results are 0.5°C (33%) warmer than the interpolated results; while this difference between the interpolated and downscaled results is potentially robust across models over the entire CCS ($p_t = 1.4 \times 10^{-2}$), the difference is not significant relative to the intermodel range in any subregions such as the central CCS. Increased heating (the S case) is sufficient to explain ΔT_{100m} in the downscaled results,

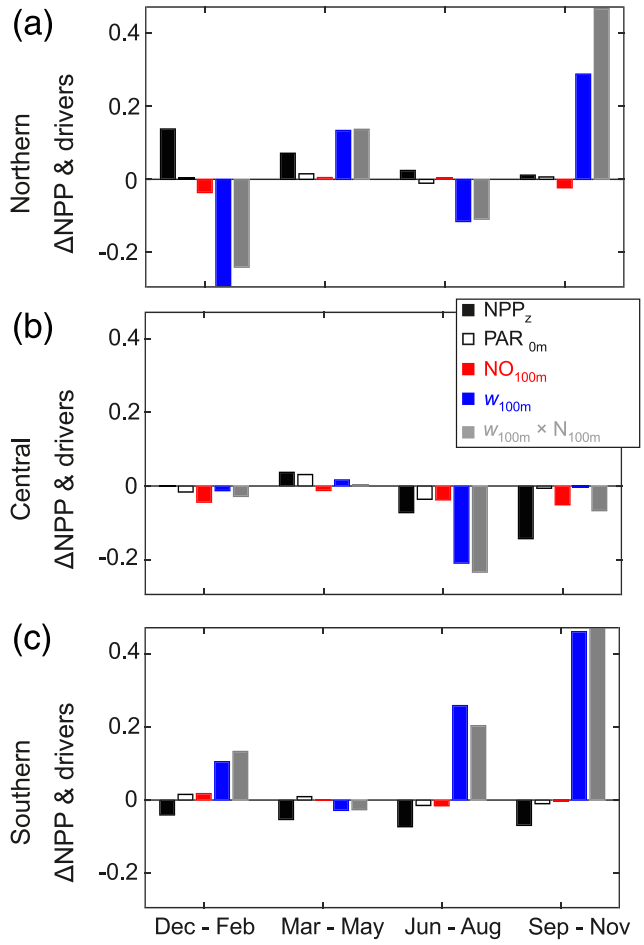

Figure 5. Fractional 2100–2000 change (Δ) in euphotic zone integrated net primary productivity (NPP_z), photosynthetically available radiation at the ocean surface (PAR_{0m}), nitrate concentrations at 100 m depth (N_{100m}), upwelling velocity at 100 m depth (w_{100m}), and the product of upwelling and nitrate concentrations at 100 m depth, an approximation of vertical advective nutrient supply. Each variable is integrated from 0–100 km offshore, and Δ is normalized to the hindcast (1994–2007) mean in each region, season, and model, then averaged across individual models and signed (larger absolute Δ is not necessarily larger relative Δ, but the absolute direction of the average change across models is preserved). Changing light (white) is, in general, more predictive of ΔNPP_z (black) than changes in vertical advective nutrient supply (gray).

with a minor cooling effect from wind changes (Figure 2b). Restricting the analysis to the nearshore areas with greatest wind stress driven upwelling slightly increases the local cooling effect from entrainment of deeper waters. Over the 0–200 km offshore coastal CCS, two thirds of the ΔT_{100m} is attributable to remote heating imported through boundary anomalies and the remaining third to heating within the CCS.

3.3. Nitrate Concentration

Downscaled ΔN_{100m} are less than 5% of the hindcast mean concentrations and vary in direction and magnitude across models (mean −0.1 mmol N m^{-3}, −2.3 to 2.3 mmol N m^{-3} range across models; Figure 3). Thus, there are no significant climate anomalies in projected N_{100m} relative to the intermodel range of the downscalings (or across the interpolated ESMs, despite large shifts in individual models). Wind (W) and stratification (S) driven changes are broadly similar in magnitude and act to increase nutrient concentrations at 100 m, while biogeochemical changes (B) counteract this effect and depress N_{100m} in most of the downscaled models. This decrease reflects basin scale vertical redistribution of NO_3^- in the ESMs, including decreased concentrations in the subpolar gyre and northern source waters of the California Current, and increased concentrations below 100 m depth in the subtropical gyre and southern source waters of the California Undercurrent; these signals propagate into the CCS at the model boundaries (Figure S8). Biogeochemical cycling along the circulation within the model domain subsequently increases N_{100m} in the 0–200 km coastal region, making the overall Δ less negative than at the model boundaries for most downscaled models. The interplay of these factors varies across ESM forcings, which diverge more than most other variables considered here. But in general, the ensemble and average SBW downscalings reflect nonlinear combinations of the S, B, and W forcing experiments (Figure 3b).

3.4. Net Primary Productivity

Changes in NPP_z follow a similar seasonal cycle and regional pattern to Δw_{50m}, peaking later at higher latitude and reaching their highest rates and seasonal variability in the central CCS (Figure 4). Like projected upwelling anomalies, ΔNPP_z is not significant compared to the intermodel range of interpolated ESMs (mean −1.0 mmol C m^{-2} y^{-1}, −3.8 to 0.9 mmol C m^{-2} y^{-1} intermodel range) or downscaled models (mean −0.8 mmol C m^{-2} y^{-1}, −3.6 to 2.1 mmol C m^{-2} y^{-1} range). There is little agreement across models with respect to the overall magnitude and direction of change over the coastal CCS. In the climate forcing experiments, the S and B forcing cases generally lead to decreased productivity in the downscaled projections, while the W forcing usually increases NPP_z. However, the full climate forcing SBW downscalings result in ΔNPP_z that is not generally a linear combination of projected changes from the individual (S, B, W) climate forcing cases (Figures 4b and 4c).

While annual-average climate anomalies are not robust across models in any subregion of the CCS, there are regionally coherent patterns of seasonal change in the ensemble results (Figure S8). In particular, the overall annual response is broadly consistent with increased productivity in the northern CCS in winter and spring, and summer and fall decreases in the central CCS, with small but consistent year-round decreases over the southern CCS (Figures 4d–4f). We evaluate whether changing PAR (at the sea surface) and nutrient supply (coarsely approximated as vertical transport of NO_3^- at 100 m depth, $w_{100m} \times N_{100m}$) are sufficient to drive seasonal, regional NPP anomalies closer to the coast (0–100 km offshore; Figure 5). On an annual average, PAR changes are small (<1%) and not significant across models, though spring increases in the central

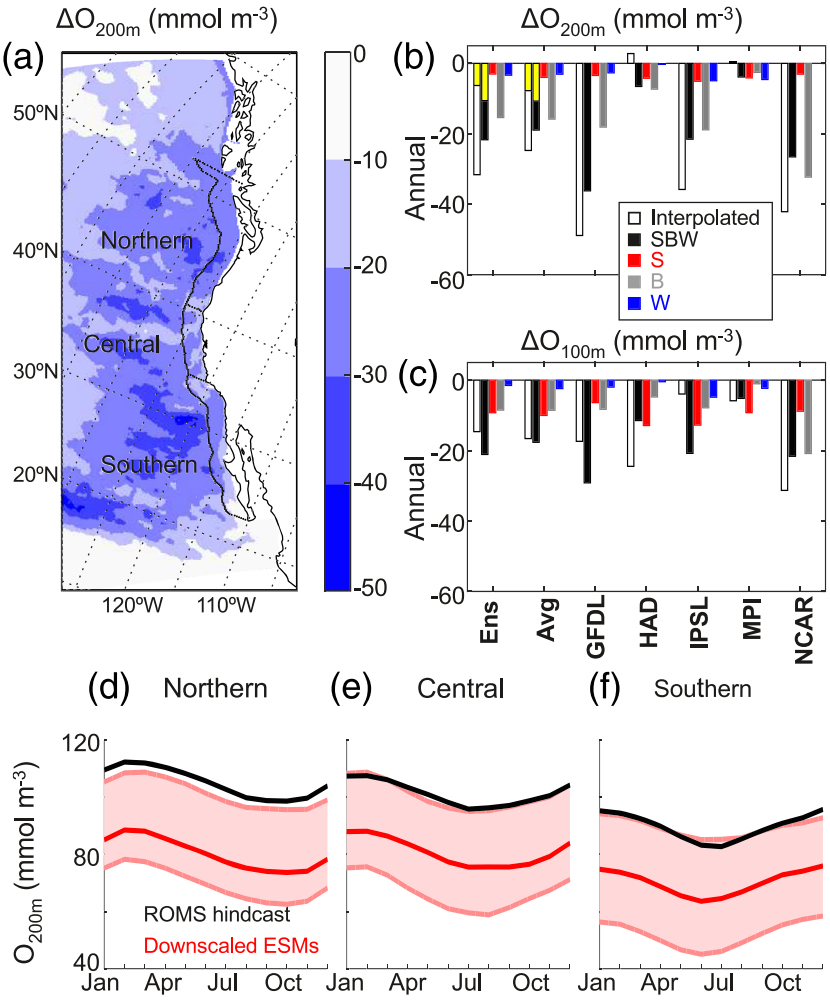

Figure 6. Oxygen concentrations at 200 m depth (O_{200m}). (a) Map of 2100–2000 change (Δ), annual average in ensemble mean forcing case. (b) Annual average 2100–2000 change (Δ), averaged over the coastal CCS, for ΔO_{200m}. The fraction of ΔO_{200m} and ΔO_{100m} attributable to changing oxygen solubility of source waters is plotted in yellow, superimposed on the interpolated 1° Earth System Models (interpolated) and full climate forcing downscalings (SBW) cases of the ensemble mean forcing response (Ens), as well as the average response across the individual models (Avg). (c) ΔO_{100m}, for comparison. At 200 m, biogeochemical boundary conditions (B) are large enough to full forcing response (SBW), while at 100 m, stratification (S) is similarly important in the overall response. Wind-driven changes (W) are small compared to the other forcings. (d–f) Regional monthly climatologies of hindcast and downscalings with full climate forcing (SBW).

CCS and summer decreases of a few percent across the CCS are coherent across models. This may represent an intensification of the existing cloud seasonality (Klein & Hartmann, 1993) driven by ocean warming and intensified surface temperature gradients in the models (Qu et al., 2014); the former suppresses low marine clouds, while the latter may enhance summertime marine fog.

In general, ΔNPP_z in the northern CCS is associated with changing light, while in the central CCS, ΔNPP_z is associated with concurrent increases and decreases in both light and nutrient supply via vertical transport. The weak sensitivities to changing light and upwelling coupled with small and variable changes in these drivers may contribute to the lack of robust NPP response across models. In the southern CCS, NPP_z does not increase with increased upwelling. Upwelling velocity and productivity are partially decoupled over the shallow continental shelf because of vertical and lateral nutrient transport by eddies (Renault, Deutsch, et al., 2016), which may contribute to this latter result. While the 12 km resolution model we use for downscaling underestimates eddy kinetic activity, partially resolved eddy activity could nonetheless contribute to

the apparent mismatch between projected changes in productivity and nutrient supply via upwelling in the southern CCS.

3.5. Oxygen Concentration

The climate driven O_2 decrease, ΔO_{200m} (Figure 6), is robust across the downscaled models (mean -19 mmol O m^{-3}, -36 to -4 mmol O m^{-3} intermodal range; $p_t = 3.6 \times 10^{-2}$). Decreases are broadly similar over the coastal CCS, though slightly larger in the northern CCS (Figures 6a and 6d). The ΔO_{200m} interpolated from the global scale models is more negative than from the downscalings (Figure 6b), while at shallower depths, ΔO is more negative in the downscalings than in the interpolated ESMs. However, those differences in magnitude of deoxygenation are never significant relative to the range of responses across models. At shallower depths, for example 100 m (Figure 6c), both interpolated and downscaled responses have significant climate anomalies (interpolated ESM mean -17 mmol O m^{-3}, -31 to -4 mmol O m^{-3} range, $p_t = 3.4 \times 10^{-2}$; downscaled mean -18 mmol O m^{-3}, -29 to -5 mmol O m^{-3} range, $p_t = 1.4 \times 10^{-2}$).

Assuming O_2 was near saturation concentrations when a water parcel was last outcropped, changing O_2 solubility of source waters can explain up to 32% of the oxygen decrease at 200 m in the interpolated ESMs and 55% of oxygen decrease in the downscalings (intermodel averages), while increased apparent oxygen utilization is inferred to account for the remainder (the solubility effect is superimposed on the ensemble and average cases in Figure 6b).

The S, B, and W climate forcing projections all decrease O_2 (Figures 6b and 6c). While the relative contribution of each set of climate forcings to the overall SBW response varies across downscaled ESMs, the changing biogeographic boundary conditions are a key contributing factor in each model, altering source water O_2 and resulting fluxes within the CCS. At 200 m depth, these changes dominate the overall response of O_2 in the coastal CCS, while wind and stratification changes are generally small contributors to the projected concentration decreases. At 100 m depth, the S and B forcing contributions are more similar, and winds remain a minor contributor.

4. Conclusions

We focus here on two key findings resulting from the downscaling of a suite of ESM climate forcings through the eddy-permitting ROMS-BEC model of the coastal CCS. First, the 2100–2000 differences in key physical and biogeochemical variables are, overall, broadly similar between the global resolution ESMs and the downscaled models. Differences remain in the hindcast and projected properties between the coarser and higher resolution models, particularly nearshore where seasonal coastal upwelling plays an important role in shaping environmental properties. But the lack of explicit incorporation of coastal processes does not prevent the ESMs from capturing major 2100–2000 climate changes, up to the 12 km model resolution explored —even for those ESMs that poorly reproduce the mean state of the CCS.

The global scale ESMs broadly agree on significant increases in temperature and decreases in oxygen in the coastal Northeast Pacific. Similarly, in the downscaled models these changes are large compared to the intermodel range, consistent across models, and of similar magnitude to the ESM results. Thus these change expectations are robust, despite less certain changes in upwelling, light, nutrients, and primary productivity. Changes in the latter variables are small compared to the intermodel range and, on an annual basis, do not shift systematically across ESMs or downscaled models; whether at a global scale or downscaled through a regional model, the magnitude of these changes derived from a single model may be idiosyncratic to the ESM chosen. For example, recent analyses of CCS nutrient changes based on climate forcings from a single ESM (the GFDL ESM2M model) have focused on how changing regional biogeochemical distributions may change nutrient concentrations and resulting nutrient supply (Rykaczewski & Dunne, 2010; Xiu et al., 2018) and the volume of low O_2 water (Dussin et al., 2019). This particular ESM forcing leads to greater increases in NO_3^- below the surface mixed layer and greater decreases in O_2 at 100–200 m than any of the other downscaled models in our analysis, suggesting that model choice could be an important factor in interpreting the results of such analyses. While the magnitude of changes in upwelling velocity, PAR, and NPP may be sensitive to model choice, in the central CCS there are nonetheless consistent seasonal shifts across both global ESMs and downscaled models. This may have important consequences for ecosystem phenology.

There is an important corollary to the dependence of NPP on divergent boundary conditions and forcings across the ESMs, and resulting uncertainty in the magnitude and direction of change for this key parameter: More realistic (complex) model ecosystem representation in the regional model will not, by itself, improve predictive skill for the climate sensitivity of NPP.

Overall, these results imply that global models with poor resolution of coastal processes nevertheless yield important information about the dominant climate impacts on the coastal CCS. Further, downscaling does not avoid the imperative to consider an ensemble of models when evaluating the robustness of future projections.

Our second key finding is that the major role of basin scale processes underlies this agreement between downscaled and global models. We find remote forcing, including regional biogeochemical redistribution and stratification, to be as or more important than the local wind changes in driving the climate response of all of the evaluated hydrographic variables—and seasonal stratification and wind-driven changes can be of similar magnitude even for upwelling velocity. Recent work has pointed to the potential importance of basin scale processes in predicting biogeochemical changes to the coastal CCS. For example, over the observational record subsurface oxygen dynamics have been closely linked to decade-scale propagation of anomalies from the North Pacific Gyre to the coastal CCS (Pozo Buil & Di Lorenzo, 2017). Basin scale processes were also found to play a key role in the projected climate response of oxygen in the CCS (Dussin et al., 2019), based on boundary conditions from one ESM and idealized wind and temperature perturbations; our analysis emphasizes that, using realistic climate forcings, this finding is broadly true across ESMs. Thus, despite the substantial body of research focused on testing the Bakun hypothesis and evaluating changes in winds, shifting winds are likely not the dominant or decisive factor controlling changes in the key biogeochemical variables in the coastal CCS that have long motivated study of the sensitivity of wind-driven upwelling to climate change.

An important caveat to these finding is that the 12 km resolution ROMS-BEC model we used does not fully resolve mesoscale or submesoscale processes that could lead to greater divergence (or convergence) of downscaled results. More highly resolved wind-ocean coupling (e.g., Renault et al., 2018; Renault, Deutsch, et al., 2016) could also play a key role in modulating the importance of local wind forcings compared to basin scale stratification and biogeochemical redistribution. PAR changes in particular are consistent with spring decreases and summer increases in marine cloud cover, the drivers and effects of which might be more robustly explored with dynamically coupled ocean-atmosphere downscalings.

Future work on changing biogeochemistry in the CCS will likely be productively focused on identifying changes that are driven by basin scale mechanisms and are robust across the range of ESMs. To the degree that projected changes are determined to be robust across multiple models (e.g., in temperature and oxygen), we found that a single ensemble-forced downscaling provides an accurate approximation of the average response across multiple downscalings and offers a low-resource option for further applications. Analysis of individual downscaled projections will still be useful in elucidating the coupling of fine scale physical and biogeochemical processes to local forcings, and demonstrating whether climate sensitivity of those processes could lead to important biogeochemical effects relative to basin scale forcings in nearshore environments. For example, one key application for future downscalings is assessing how local pollution sources such as urban wastewater affect regional responses to changing climate.

Conflict of Interests

The authors declare no conflicts of interest.

Data and Materials Availability

Codes used for model simulations are available online (https://github.com/UCLA-ROMS/Code). The ROMS-BEC model outputs presented in this work are archived at the Dryad Digital Repository (https://doi.org/10.5061/dryad.xsj3tx9d5). CMIP5 model outputs are accessible via the Earth System Grid Federation data portal (https://esgf-node.llnl.gov).

Acknowledgments

We thank the many individuals who have contributed to the publicly accessible databases and climate models referenced herein, as well as two anonymous reviewers for their thoughtful and constructive comments to improve this manuscript. This work used computing resources from Cheyenne at NCAR's Computational and Information Systems Laboratory, and the Engineering Discovery Environment (XSEDE). Funding was provided by the following grants: National Science Foundation (NSF) OCE-1635632 and OCE-1847687 to D. B.; NOAA NA15NOS47801-86, NA15NOS47801-92, and NA18NOS47801-67, NSF OCE-1419323 and OCE-1737282, California Sea Grant and Ocean Protection Council R/OPCOAH-1, and Gordon and Betty Moore Foundation GBMF#3775 awarded to C. D.; NSF OCE-1419450 to L. R.

References

Adams, K. A., Barth, J. A., & Chan, F. (2013). Temporal variability of near-bottom dissolved oxygen during upwelling off central Oregon. *Journal of Geophysical Research: Oceans*, *118*, 4839–4854. https://doi.org/10.1002/jgrc.20361

Alexander, M. A., Scott, J. D., Friedland, K. D., Mills, K. A., Nye, J. A., Pershing, A. J., & Thomas, A. C. (2018). Projected sea surface temperatures over the 21st century: Changes in the mean, variability, and extremes for large marine ecosystem regions of northern oceans. *Elem Sci Anth*, *6*(1), 9. https://doi.org/10.1525/elementa.191

Arora, V. K., & Boer, G. J. (2001). Effects of simulated climate change on the hydrology of major river basins. *Journal of Geophysical Research*, *106*(D4), 3335–3348. https://doi.org/10.1029/2000JD900620

Bakun, A. (1990). Global climate change and intensification of coastal ocean upwelling. *Science*, *247*(4939), 198–201. https://doi.org/10.1126/science.247.4939.198

Bakun, A., Black, B. A., Bograd, S. J., García-Reyes, M., Miller, A. J., Rykaczewski, R. R., & Sydeman, W. J. (2015). Anticipated effects of climate change on coastal upwelling ecosystems. *Current Climate Change Reports*, *1*(2), 85–93. https://doi.org/10.1007/s40641-015-0008-4

Brady, R. X., Alexander, M. A., Lovenduski, N. S., & Rykaczewski, R. R. (2017). Emergent anthropogenic trends in California Current upwelling. *Geophysical Research Letters*, *44*, 5044–5052. https://doi.org/10.1002/2017GL072945

Capet, X., McWilliams, J. C., Molemaker, M. J., & Shchepetkin, A. F. (2008). Mesoscale to submesoscale transition in the California Current System. Part II: Frontal processes. *Journal of Physical Oceanography*, *38*(1), 44–64. https://doi.org/10.1175/2007jpo3672.1

Capotandi, A., Alexander, M. A., Bond, N. A., Curchitser, E. N., & Scott, J. D. (2012). Enhanced upper ocean stratification with climate change in the CMIP3 models. *Journal of Geophysical Research*, *117*, C04031. https://doi.org/10.1029/2011JC007409

Chan, F., Barth, J. A., Lubchenco, J., Kirincich, A., Weeks, H., Peterson, W. T., & Menge, B. A. (2008). Emergence of anoxia in the California Current Large Marine Ecosystem. *Science*, *319*(5865), 920. https://doi.org/10.1126/science.1149016

Dai, A., Qian, T., Trenberth, K. E., & Milliman, J. D. (2009). Changes in continental freshwater discharge from 1948 to 2004. *Journal of Climate*, *22*(10), 2773–2792. https://doi.org/10.1175/2008JCLI2592.1

Davis, K. A., Banas, N. S., Giddings, S. N., Siedlecki, S. A., MacCready, P., Lessard, E. J., et al. (2014). Estuary-enhanced upwelling of marine nutrients fuels coastal productivity in the U.S. Pacific Northwest. *Journal of Geophysical Research: Oceans*, *119*, 8778–8799. https://doi.org/10.1002/2014JC010248

Deutsch, C., Frenzel, H., McWilliams, J.C., Renault, L., Kessouri, F., Howard, E., et al. (2020). *Biogeochemical variability in the California Current System*. Preprint on BioRxiv: https://www.biorxiv.org/content/10.1101/2020.02.10.942565v1

Di Lorenzo, E., Miller, A. J., Schneider, N., & McWilliams, J. C. (2005). The warming of the California Current System: Dynamics and ecosystem implications. *Journal of Physical Oceanography*, *35*(3), 336–362. https://doi.org/10.1175/JPO-2690.1

Dussin, R., Curchitser, E. N., Stock, C. A., & Van Oostende, N. (2019). Biogeochemical drivers of changing hypoxia in the California Current Ecosystem. *Deep Sea Research Part II: Topical Studies in Oceanography*, *169-170*, 104590. https://doi.org/10.1016/j.dsr2.2019.05.013

Fabry, V. J., Seibel, B. A., Feely, R. A., & Orr, J. C. (2008). Impacts of ocean acidification on marine fauna and ecosystem processes. *ICES Journal of Marine Science*, *65*(3), 414–432. https://doi.org/10.1093/icesjms/fsn048

Feely, R. A., Sabine, C. L., Hernandez-Ayon, J. M., Ianson, D., & Hales, B. (2008). Evidence for upwelling of corrosive "acidified" water onto the continental shelf. *Science*, *320*(5882), 1490–1492. https://doi.org/10.1126/science.1155676

Ferrari, M. R., Miller, J. R., & Russell, G. L. (2007). Modeling changes in summer temepratrue of the Fraser River during the next century. *Journal of Hydrology*, *342*(3–4), 336–346. https://doi.org/10.1016/j.jhydrol.2007.06.002

Garcia, H. E., Locarnini, R. A., Boyer, T. P., Antonov, J. I., Baranova, O. K., Zweng, M. M., et al. (2013a). Volume 3: Dissolved oxygen, apparent oxygen utilization, and oxygen saturation. In S. Levitus, & A. Mishonov (Eds.), *World Ocean Atlas 2013* (U.S. Department of Commerce National Oceanic and Atmospheric Administration Atlas NESDIS-75). Silver Spring, MD: National Oceanographic Data Center. Retrieved from https://www.nodc.noaa.gov/OC5/woa13/

Garcia, H. E., Locarnini, R. A., Boyer, T. P., Antonov, J. I., Baranova, O. K., Zweng, M. M., et al. (2013b). Volume 4: Dissolved inorganic nutrients (phosphate, nitrate, silicate). In S. Levitus & A. Mishonov (Eds.), *World Ocean Atlas 2013* (U.S. Department of Commerce National Oceanic and Atmospheric Administration Atlas NESDIS-76). Silver Spring, MD: National Oceanographic Data Center. Retrieved from https://www.nodc.noaa.gov/OC5/woa13/

García-Reyes, M., Sydeman, W. J., Schoeman, D. S., Rykaczewski, R. R., Black, B. A., Smit, A. J., & Bograd, S. J. (2015). Under pressure: Climate change, upwelling, and eastern boundary upwelling ecosystems. *Frontiers in Marine Science*, *2*, 109. https://doi.org/10.3389/fmars.2015.00109

Gómez-Valdivia, F., Parés-Sierra, A., & Flores-Morales, A. L. (2015). The Mexican Coastal Current: A subsurface seasonal bridge that connects the tropical and subtropical Northeastern Pacific. *Contintental Shelf Research*, *110*, 100–107. https://doi.org/10.1016/j.csr.2015.10.010

Gould, R. W., Ko, D. S., Ladner, S. D., Lawson, T. A., & MacDonald, C. P. (2019). Comparison of satellite, model, and *in situ* values of photosyntethically available radiation (PAR). *Journal of Atmospheric and Oceanic Technology*, *36*(4), 535–555. https://doi.org/10.1175/JTECH-D-18-0096.1

Gruber, N., Hauri, C., Lachkar, Z., Loher, D., Frölicher, T. L., & Plattner, G.-K. (2012). Rapid progression of ocean acidification in the California Current System. *Science*, *337*(6091), 220–223. https://doi.org/10.1126/science.1216773

Gruber, N., Lachkar, Z., Frenzel, H., Marchesiello, P., Münnich, M., McWilliams, J. C., et al. (2011). Eddy-induced reduction of biological production in eastern boundary upwelling systems. *Nature Geoscience*, *4*(11), 787–792. https://doi.org/10.1038/ngeo1273

Harvey, C., Garfield, N., Williams, G., Andrews, K., Barceló, C., Barnas, K., et al. (2017). *Ecosystem status report of the California Current for 2017* (U.S. Department of Commerce National Oceanic and Atmospheric Administration Technical Memorandum NMFS-NWFSC-139). Seattle, WA: Northwest Fisheries Science Center. https://doi.org/10.7289/V5/TM-NWFSC-139

Hauri, C., Gruber, N., Vogt, M., Doney, S. C., Feely, R. A., Lachkar, Z., et al. (2013). Spatiotemporal variability and long-term trends of ocean acidification in the California Current System. *Biogeosciences*, *10*(1), 193–216. https://doi.org/10.5194/bg-10-193-2013

Howard, E. M., Penn, J. L., Frenzel, H., Seibel, B. A., Bianchi, D., Renault, L., et al. (2020). Climate driven aerobic habitat loss in the California Current System. *Science Advances*, *6*(20), eaay3188. https://doi.org/10.1126/sciadv.aay3188

Keller, A. A., Ciannelli, L., Wakefield, W. W., Simon, V., Barth, J. A., & Pierce, S. D. (2017). Species-specific responses of demersal fishes to near-bottom oxygen levels within the California Current large marine ecosystem. *Marine Ecology Progress Series*, *568*, 151–173. https://doi.org/10.3354/meps12066

Kessouri, F., Bianchi, D., Renault, L., McWilliams, J. C., Frenzel, H., & Deutsch, C. (2020). Submesoscale currents modulate the seasonal cycle of nutrients and productivity in the California Current System. *Global Biogeochemical Cycles*. https://doi.org/10.1029/2020GB006578

Klein, S. A., & Hartmann, D. L. (1993). The seasonal cycle of low stratiform clouds. *Journal of Climate*, *6*(8), 1587–1606. https://doi.org/10.1175/1520-0442(1993)006<1587:TSCOLS>2.0.CO;2

Koslow, J. A., Goericke, R., Lara-Lopez, A., & Watson, W. (2011). Impact of declining intermediate-water oxygen on deepwater fishes in the California current. *Marine Ecology Progress Series*, *436*, 207–218. https://doi.org/10.3354/meps09270

Large, W. B. (2006). Surface fluxes for practitioners of global ocean data assimilation. In E. P. Chassignet & J. Verron (Eds.), *Ocean weather forecasting*. Dordrecht, Netherlands: Springer. https://doi.org/10.1007/1-4020-4028-8

Levin, P. S., & Schwing, F. B. (Eds) (2011). *Technical background for an integrated ecosystem assessment of the California Current* (U.S. Department of Commerce National Oceanic and Atmospheric Administration Technical Memorandum NMFS-NWFSC-139). Seattle, WA: Northwest Fisheries Science Center. Retrieved from https://www.nwfsc.noaa.gov/publications

Li, Q. P., Franks, P. J. S., Ohman, M. D., & Landry, M. R. (2012). Enhanced nitrated fluxes and biological processes at a frontal zone in the southern California current system. *Journal of Plankton Research*, *34*(9), 790–801. https://doi.org/10.1093/plankt/fbs006

Locarnini, R. A., Mishonov, A. V., Antonoy, J. I., Boyer, T. P., Garcia, H. E., Baranova, M. M., et al. (2013). Volume 1: Temperature. In S. Levitus, & A. Mishonov (Eds.), *World Ocean Atlas 2013* (U.S. Department of Commerce National Oceanic and Atmospheric Administration Atlas NESDIS-73). Silver Spring, MD: National Oceanographic Data Center. Retrieved from https://www.nodc.noaa.gov/OC5/woa13/

Long, M. C., Deutsch, C., & Ito, T. (2016). Finding forced trends in oceanic oxygen. *Global Biogeochemical Cycles*, *30*, 381–397. https://doi.org/10.1002/2015GB005310

Lynn, R. J., & Simpson, J. J. (1987). The California Current System: The seasonal variability of its physical characteristics. *Journal of Geophysical Research*, *92*, 12,947–12,966. https://doi.org/10.1029/JC092iC12p12947

MacCready, P., Banas, N. S., Hickey, B. M., Dever, E. P., & Liu, Y. (2009). A model study of tide- and wind-induced mixing in the Columbia River Estuary and plume. *Continental Shelf Research*, *29*(1), 278–291. https://doi.org/10.1016/j.csr.2008.03.015

Moore, J. K., Doney, S. C., Kleypas, J. A., Glover, D. M., & Fung, I. Y. (2002). An intermediate complexity marine ecosystem model for the global domain. *Deep Sea Research Part II: Topical Studies in Oceanography*, *49*(3), 403–462. https://doi.org/10.1016/S0967-0645(01)00108-4

Morrison, J., Quick, M. C., & Foreman, M. G. G. (2002). Climate change in the Fraser River watershed: Flow and temperature projections. *Journal of Hydrology*, *263*(1–4), 230–244. https://doi.org/10.1016/S0022-1694(02)00065-3

Nagai, T., Gruber, N., Frenzel, H., Lachkar, Z., McWilliams, J. C., & Plattner, G.-K. (2015). Dominant role of eddies and filaments in the offshore transport of carbon and nutrients in the California Current System. *Journal of Geophysical Research: Oceans*, *120*, 5318–5341. https://doi.org/10.1002/2015JC010889

Naik, P. K., & Jay, D. A. (2011). Distinguishing human and climate influences on the Columbia River: Changes in mean flow and sediment transport. *Journal of Hydrology*, *404*(3–4), 259–277. https://doi.org/10.1016/j.jhydrol.2011.04.035

Pozo Buil, M., & Di Lorenzo, E. (2017). Decadal dynamics and predictability of oxygen and subsurface tracers in the California Current System. *Geophysical Research Letters*, *44*, 4204–4213. https://doi.org/10.1002/2017GL072931

Pytlak, E., Frans, C., Duffy, K., Johnson, J., Nijssen, B., Chegwidden, O., & Rupp, D. (2018). Part I: Hydroclimate projections and analyses. In D. Donnell, & S. Williams (Eds.), *Climate and hydrology datasets for River Management Joint Operating Committee long-term planning studies: Second Edition* (U.S. Department of Energy, Bonneville Power Administration report RMJOC-II). Portland, OR: Bonneville Power Administration. Retrieved from https://www.bpa.gov/p/Generation/Hydro/Pages/Climate-Change-FCRPS-Hydro.aspx

Qu, X., Hall, A., Klein, S. A., & Caldwell, P. M. (2014). On the spread of changes in marine low cloud cover in climate model simulations of the 21st century. *Climate Dynamics*, *42*, 2603–2626. https://doi.org/10.1007/s00382-013-1945-z

Renault, L., Deutsch, C., McWilliams, J. C., Frenzel, H., Liang, J.-H., & Colas, F. (2016). Partial decoupling of primary productivity from upwelling in the California Current System. *Nature Geoscience*, *9*(7), 505–508. https://doi.org/10.1038/ngeo2722

Renault, L., Hall, A., & McWilliams, J. C. (2016). Orographic shaping of UW West Coast wind profiles during the upwelling season. *Climate Dynamics*, *46*(1–2), 273–289. https://doi.org/10.1007/s00382-015-2583-4

Renault, L., McWilliams, J. C., & Gula, J. (2018). Dampening of submesoscale currents by air-sea stress coupling in the Californian Upwelling System. *Scientific Reports*, *8*(1), 13388. https://doi.org/10.1038/s41598-018-31602-3

Renault, L., McWilliams, J.C., Jousse, A., Deutsch, C., Frenzel, H., Kessouri, F., & Chen, R. (2020). *The physical structure and behavior of the California Current System*. Preprint on BioRxiv: https://www.biorxiv.org/content/10.1101/2020.02.10.942730v1

Renault, L., McWilliams, J. C., & Masson, S. (2017). Satellite observations of imprint of oceanic current on wind stress by air-sea coupling. *Scientific Reports*, *7*(1), 17747. https://doi.org/10.1038/s41598-017-17939-1

Renault, L., Molemaker, M. J., McWilliams, J. C., & Schepetkin, A. F. (2016). Modulation of wind work by oceanic current interaction with the atmosphere. *Journal of Physical Oceanography*, *46*(6), 1685–1704. https://doi.org/10.1175/JPO-D-15-0232.1

Rykaczewski, R. R., & Dunne, J. P. (2010). Enhanced nutrient supply to the California Current Ecosystem with global warming and increased stratification in an Earth System Model. *Geophysical Research Letters*, *37*, L21606. https://doi.org/10.1029/2010GL045019

Rykaczewski, R. R., Dunne, J. P., Sydeman, W. J., García-Reyes, M., Black, B. A., & Bograd, S. J. (2015). Poleward displacement of coastal upwelling-favorable winds in the ocean's eastern boundary currents through the 21st century. *Geophysical Research Letters*, *42*, 6424–6431. https://doi.org/10.1002/2015GL064694

Shchepetkin, A. F., & McWilliams, J. C. (2005). The regional oceanic modeling system (ROMS): A split-explicit, free-surface, topography-following-coordinate oceanic model. *Ocean Model*, *9*(4), 347–404. https://doi.org/10.1016/j.ocemod.2004.08.002

Siedlecki, S. A., Banas, N. S., Davis, K. A., Giddings, S., Hickey, B. M., MacCready, P., et al. (2014). Seasonal and interannual oxygen variability on the Washington and Oregon continental shelves. *Journal of Geophysical Research: Oceans*, *120*, 608–633. https://doi.org/10.1002/2014JC010254

Skamarock, W. C., Klemp, J. B., Dudhia, J., Gill, D. O., Barker, D., Duda, M. G., & Powers, J. G. (2008). *A description of the advanced research WRF version 3. (National Center for Atmospheric Research Technical Note NCAR/TN-475+STR)*. Boulder, CO: University Corporation for Atmospheric Research. https://doi.org/10.5065/D68S4MVH

Sydeman, W. J., Thompson, S. A., Field, J. C., Peterson, W. T., Tanasichuk, R. W., Freeland, H. J., et al. (2011). Does positioning of the North Pacific Current affect downstream ecosystem productivity? *Geophysical Researhc Letters*, *38*, L12606. https://doi.org/10.1029/2011GL047212

Sydeman, W. J., García-Reyes, M., Schoeman, D. S., Rykaczewski, R. R., Thompson, S. A., Black, B. A., & Bograd, S. J. (2014). Climate change and wind intensification in coastal upwelling ecosystems. *Science*, *345*(6192), 77–80. https://doi.org/10.1126/science.1251635

Taylor, K. E., Stouffer, R. J., & Meehl, G. A. (2012). An overview of CMIP5 and the experiment design. *Bulletin of the American Meteorological Society*, *93*(4), 485–498. https://doi.org/10.1175/BAMS-D-11-00094.1

Wang, D., Guhier, T. C., Menge, B. A., & Ganguly, A. R. (2015). Intensification and spatial homogenization of coastal upwelling under climate change. *Nature*, *518*(7539), 390–394. https://doi.org/10.1038/nature14235

Xiu, P., Chai, F., Curchitser, E. N., & Castruccio, F. S. (2018). Future changes in coastal upwelling ecosystem with global warming: The case of the California Current System. *Scientific Reports*, *8*(1), 2866. https://doi.org/10.1038/s41598-018-21247-7

Zweng, M. M., Reagan, J. R., Antonoy, J. I., Locarnini, R. A., Mishonov, A. V., Boyer, T. P., et al. (2013). Volume 2: Salinity. In S. Levitus & A. Mishonov (Eds.), *World Ocean Atlas 2013* (U.S. Department of Commerce National Oceanic and Atmospheric Administration Atlas NESDIS-74). Silver Spring, MD: National Oceanographic Data Center. Retrieved from https://www.nodc.noaa.gov/OC5/woa13/